Astron. Astrophys. 345, 841–846 (1999)

ASTRONOMY AND ASTROPHYSICS

The carbon star IRAS 15194-5115: circumstellar CO radio and FIR rotational lines⋆

N. Ryde[1], **F.L. Schöier**[2], **and H. Olofsson**[2]

[1] Uppsala Astronomical Observatory, Box 515, S-751 20 Uppsala, Sweden
[2] Stockholm Observatory, S-133 36 Saltsjöbaden, Sweden

Received 15 January 1999 / Accepted 2 March 1999

Abstract. We have modelled radio and far-infrared rotational lines of ^{12}CO and ^{13}CO obtained from the circumstellar envelope of the infrared-bright carbon star IRAS 15194-5115. Eleven rotational lines between J=1–0 and 21–20 and nine rotational lines between J=1–0 and 22–21 in the ground vibrational states of ^{12}CO and ^{13}CO, respectively, provide the observational constraints. A model of the circumstellar envelope with a constant mass-loss rate (1×10^{-5} M$_\odot$ yr^{-1}) and ^{12}CO/^{13}CO-ratio (5.5) is consistent with our observed FIR and radio data, suggesting that the wind characteristics have not changed significantly over the past few thousand years. Thus, IRAS 15194-5115 appears to be a highly evolved AGB-star, but the carbon star properties combined with the inferred low ^{12}C/^{13}C-ratio make the evolutionary status of this star uncertain. It may have been a J-star for which the ^{12}C/^{13}C-ratio has remained low, or it may be a star of 5 to 8 solar masses, which has recently become a carbon star due to quenching of hot bottom burning. The dust properties or the relative amount of dust in the envelope appear to be different from those in the envelope of the well known carbon star IRC+10 216.

Key words: stars: AGB and post-AGB – stars: circumstellar matter – stars: individual: IRAS15194-5115 – stars: late-type – infrared: stars

1. Introduction

Red giant stars lose large amounts of matter through a massive, but slow, stellar wind during their late evolution on the Asymptotic Giant Branch (AGB). The mass loss results in circumstellar envelopes (CSEs), several thousand stellar radii in size, consisting of gas, mainly in molecular form, and dust. Important information on late stellar evolution can be obtained from the circumstellar emission (Olofsson 1996).

We have studied the third brightest (at 12 μm) carbon star (C-star) IRAS 15194-5115 (or II Lup), which is the brightest one known in the southern hemisphere, in several rotational transitions in the ground vibrational states of ^{12}CO and ^{13}CO. The lowest energy lines, J=1–0 etc., lie at radio wavelengths and probe the outer regions of the CSE. Higher energy lines, for example, the J=14–13 to J=22–21 lines presented in this paper, which lie in the far-infrared (FIR) wavelength range 100–200 μm originate from regions much closer to the star. By combining observations in these two wavelength ranges we are able to probe different regions of the CSE, and to compare wind characteristics, such as mass loss rate, and molecular abundances (including isotope ratios), over a time span of several thousand years.

IRAS 15194-5115 was discovered by Epchtein et al. (1987; the ESO-Valinhos 2.2 μm sky survey) and by IRAS in the far-infrared, and it was identified as a C-star using optical and infrared spectra (Meadows et al. 1987). To understand the late evolutionary phases of C-stars, in which they undergo intense mass loss, this star provides an object which is bright enough to make possible an exhaustive spectroscopic investigation over a broad range of wavelengths. IRAS 15194-5115 shows similarities in the infrared to the well-studied prototype C-star IRC+10 216 (Meadows et al. 1987; Lopez et al. 1993). On the basis of radio observations Nyman et al. (1993) concluded that most molecular species, except a few, have circumstellar abundances comparable to those in IRC+10 216. Also, they found that the two objects have comparable mass loss rates. The most striking difference between these two C-stars is the ^{12}C/^{13}C-ratio, which appears to be at least five times lower in IRAS 15194-5115 (Nyman et al. 1993).

Here, we present observations of FIR rotational lines of ^{12}CO and ^{13}CO from IRAS 15194-5115, as well as a model interpreting these data and radio rotational lines.

2. Observations

We have obtained FIR observations with the Infrared Space Observatory (Kessler et al. 1996), see Fig. 1. The Long Wavelength Spectrometer (LWS, Clegg et al. 1996), with a beam size assumed to be $70''$, was used in the grating mode (LWS01), covering the range 90-197 μm, and providing a mean spectral resolution element of $\sim$0.7 μm (this corresponds to $\mathrm{R} = \lambda/\Delta\lambda \sim 100$–$250$; hence the circumstellar lines are far

Send offprint requests to: N. Ryde (ryde@astro.uu.se)

⋆ Based on observations with ISO, an ESA project with instruments funded by ESA Member States (especially the PI countries: France, Germany, the Netherlands and the United Kingdom) and with the participation of ISAS and NASA.

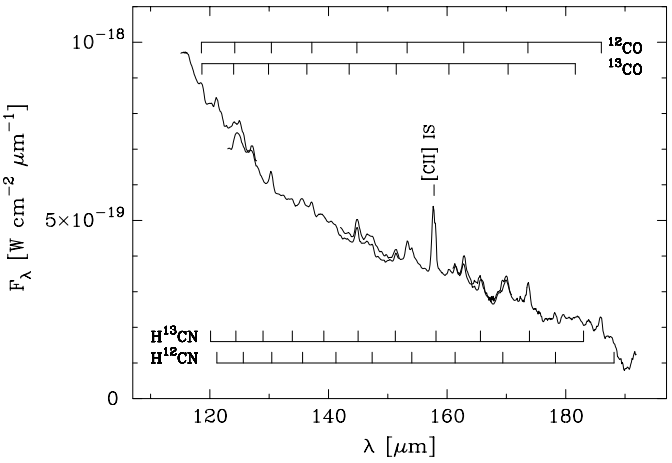

Fig. 1. The FIR spectrum of IRAS 15194-5115 as observed by the ISO satellite. Fluxes from four detectors are shown without scaling. The overlap regions show the uncertainties, both the relative and the absolute ones, in these ISO-LWS observations. All rotational transitions within the ground vibrational states of ^{12}CO, ^{13}CO, H^{12}CN, and H^{13}CN in this region are indicated. Also the interstellar [CII] line is marked. These emission lines are superimposed on the continuum emitted by the dust around the star

Table 1. Observed and modelled CO FIR rotational lines from IRAS 15194-5115. A colon (:) marks lines with uncertain flux estimates due to a complex continuum around the line around 143.5μm or due to a blending of two or three lines of ^{12}CO, ^{13}CO or HCN

$\lambda_{\rm obs}$ [μm]	$F_{\rm obs}$ [W cm^{-2}]	Transition	$\lambda_{\rm vac}$ [μm]	$F_{\rm mod}$ [W cm^{-2}]
185.99	3.0×10^{-20}	CO(14–13)	185.999	2.2×10^{-20}
181.61	1.3×10^{-20}	^{13}CO(15–14)	181.608	7.6×10^{-21}
173.66	3.8×10^{-20}	CO(15–14)	173.631	2.3×10^{-20}
162.85	4.2×10^{-20}	CO(16–15)	162.811	2.5×10^{-20}
160.54	1.5×10^{-20}	^{13}CO(17–16)	160.305	8.6×10^{-21}
153.38	4.0×10^{-20}	CO(17–16)	153.267	2.6×10^{-20}
151.37	1.2×10^{-20}	^{13}CO(18–17)	151.431	9.1×10^{-21}
144.80	3.8×10^{-20}	CO(18–17)	144.784	2.7×10^{-20}
143.40	6.2×10^{-21} :	^{13}CO(19–18)	143.493	9.5×10^{-21}
137.12	3.5×10^{-20}	CO(19–18)	137.196	2.9×10^{-20}
136.35	1.5×10^{-20}	^{13}CO(20–19)	136.352	1.0×10^{-20}
130.28	1.9×10^{-20} :	CO(20–19)	130.369	3.0×10^{-20}
129.83	6.2×10^{-21} :	^{13}CO(21–20)	129.891	1.0×10^{-20}
124.10	2.8×10^{-20} :	CO(21–20)	124.193	3.1×10^{-20}
124.10	9.3×10^{-21} :	^{13}CO(22–21)	124.019	1.1×10^{-20}

from being resolved). The spectra were sampled at 0.15 μm. The 3.5$^{\rm h}$ of observations were performed on 19 September 1997 during ISO revolution 674. The reductions were made using the most recent pipeline basic reduction package OLP (v.7) and the ISO Spectral Analysis Package (ISAP v.1.5). The pipeline processing of the data, such as wavelength and flux calibration, is described in Swinyard et al. (1996); the combined absolute and systematic uncertainties in the fluxes are of the order of $\pm$30%. The accuracy of the wavelength varies and can be as bad as $\pm$0.1 μm. The observed fluxes are measured after scaling the four detectors and averaging the two measurements in the overlap regions between different LWS detectors. The scaling needed is at most a few percent. In Fig. 1 the fluxes from the four detectors are shown without any scaling. Additional uncertainties in the line fluxes, sometimes large, are introduced in the continuum subtraction. A dust continuum level is estimated and subtracted over a limited wavelength interval, usually $\sim$10 μm. The errors in the fluxes due to the uncertain continuum subtraction are estimated to be around $\pm$20%. A few CO-lines are blended by an unknown amount of H^{13}CN, leading to somewhat too high measured CO-fluxes in these lines.

Our final LWS spectrum is dominated by thermal radiation due to the large quantity of dust around the object. The dust modelling of the object by Lopez et al. (1993) shows that for wavelengths longer than 10 μm the spectrum is totally dominated by dust emission. Superimposed on this emission are molecular emission lines, of which we have identified those due to ^{12}CO, ^{13}CO, and H^{12}CN (all relevant rotational transitions within the ground vibrational states of ^{12}CO, ^{13}CO, H^{12}CN, and H^{13}CN are indicated in Fig. 1). Here we present eight lines between J=14–13 to 21–20 of ^{12}CO and seven lines between J=15–14 and 22–21 of ^{13}CO, Table 1 and Fig. 3. A similar LWS spectrum of IRC+10 216 has been presented by Cernicharo et al. (1996). The observed fluxes from this source are an order of magnitude higher than those towards IRAS 15194-5115, making the analysis more difficult in our case.

As a supplement to the ISO data, we have used ^{12}CO and ^{13}CO radio-line observations from SEST [Swedish-ESO Submillimetre Telescope; the J=1–0 and 2–1 spectra published in Nyman et al. (1993), and a ^{12}CO(3–2) spectrum (Nyman, private communication)]. The radio data are presented in Fig. 2. The errors in the radio intensities are about $\pm$10%, and the resolution is better than 1 km s^{-1}.

3. The model

In order to model the circumstellar emission lines we have used a numerical simulation code, based on the Monte Carlo method, to solve the non-LTE radiative transfer of ^{12}CO and ^{13}CO taking into account 30 rotational levels for each of the ground and first vibrational states (see Schöier, PhD thesis in prep., for details). Using 40 energy levels does not change the temperature structure and the line intensities noticeably. For example, in the innermost regions, cooling by CO excited to higher levels than J=20–25 are unimportant. Crosas & Menten (1997) also found that around 30 levels are sufficient to treat the CO cooling in CSEs properly. The decline in CO cooling in the inner regions of the CSE, as demonstrated in Fig. 4, is due to the fact that the CO lines become optically thick.

The transition probabilities and energy levels are taken from Chandra et al. (1996), and the rotational (CO-H_2) collisional rate coefficients are from Flower & Launay (1985) (they are extrapolated for $J>11$ and for temperatures higher than 250 K). The derived intensities of the FIR lines are not very sensitive to the accuracy of this extrapolation since they are formed in LTE

(see below). Collisional transitions between vibrational levels are not important due to the low density and the short radiative lifetimes.

The kinetic gas temperature is calculated in a self-consistent way, using the derived level populations, by solving the energy balance equation (e.g. Goldreich & Scoville 1976),

$$\frac{dT}{dr} = (2-2\gamma)\frac{T}{r} + \frac{\gamma-1}{n_{\rm H_2} k v_\infty}(H-C), \quad (1)$$

where γ is the adiabatic index, $n_{\rm H_2}$ the number density of molecular hydrogen which is the most abundant species in the CSE, v_∞ the terminal gas expansion velocity, k the Boltzmann constant, H the total heating rate per unit volume, and C the total cooling rate per unit volume.

The first term on the right-hand-side in the energy balance equation is the cooling due to the adiabatic expansion of the gas. The adiabatic index, i.e. the ratio of the specific heats $\gamma = {\rm c_p}/{\rm c_v}$, can be assumed to be 5/3 since H_2 can be treated as a 'monoatomic gas'. This is true as long as the corrections on γ due to rotational excitation of H_2 are small. These corrections are important for temperatures greater than approximately 300 K, i.e. for the innermost regions where γ=7/5 (Goldreich & Scoville 1976). According to our tests, the effect of a varied adiabatic index (in comparison to a constant one) is only a few percent in the intensities, which is in agreement with the result of Groenewegen (1994).

Additional cooling is provided by emission from the molecules CO and H_2. The molecular cooling due to CO (^{12}CO and ^{13}CO) is calculated from the derived level populations using the expression of Crosas & Menten (1997). For H_2 we use the approach by Groenewegen (1994). HCN could be an important coolant in the inner parts of the envelope (Cernicharo et al. 1996), but Groenewegen (1994) demonstrates that HCN cooling is only of minor importance. In the present version of the code HCN cooling is therefore not included.

The heating is assumed to be dominated by dust-gas collisions (Groenewegen 1994) and the photoelectric effect (Crosas & Menten 1997). In the former case a number of free parameters describing the dust are introduced. These are highly uncertain but affect the derived line intensities. Here we assume that the Q-parameter, i.e., the efficiency of momentum transfer, to be equal to 0.03, and define a new parameter that contains the other dust parameters, $h = (\Psi/0.01)(2.0\,{\rm g\,cm^{-3}}/\rho_{\rm d})(0.05\,\mu{\rm m}/a_{\rm d})$, where Ψ is the gas-to-dust ratio, $\rho_{\rm d}$ is the dust density, and $a_{\rm d}$ the mean size of the dust particles. The normalised values are the ones we used to fit the CO line emission of IRC+10 216 using our model (see Schöier et al. in prep.). Heating (or cooling) due to a temperature difference (heat exchange) between the dust and the gas could affect the derived temperature structure of the gas and hence the line intensities, especially in the inner parts where the coupling between dust and gas is high. However, using the dust temperature structure for IRAS 15194-5115 from Lopez et al. (1993) and the analytical expression from Groenewegen (1994), we conclude that this effect is only of minor importance.

IRAS 15194-5115 is a LPV with a period of 580 days, and with a variation of $0.8^{\rm mag}$ in the Johnson M filter (Le Bertre, 1992), but the amplitude decreases rapidly towards longer wavelengths. The period-luminosity relation for C-stars (Groenewegen & Whitelock 1996) gives a luminosity of 8770 $L_\odot$. Using this luminosity and the apparent bolometric flux we arrive at a distance of 600 pc, a value in agreement with the ones discussed recently in the literature. The stellar temperature is set to $T_{\rm eff} = 2200$ K, a value typical for C-stars with a high mass loss rate (e.g., Le Bertre 1997). However, the mass loss rate derived is quite insensitive to the choice of $T_{\rm eff}$, since radiative excitation is of very little importance in this case. The reason is that, as our calculations show, in this high-density CSE the populations in the CO rotational levels are determined by collisions, and hence the kinetic temperature, out to a few$\times 10^{16}$ cm (Fig. 4). Consequently, the light variability of the object is also unimportant for the excitation. In the present version of our code only the star provides radiation since no thermal emission from dust in the CSE is included. This latter radiation could be significant for pumping vibrational states, leading to non-thermal level populations of the rotational states which could effect the FIR line intensities, but this effect is judged to be small in this high-density CSE.

We assume a spherically symmetric CSE formed by a constant mass loss rate and expanding at a constant velocity. From the widths of the radio lines we are able to estimate the terminal gas expansion velocity, $\sim$21.5 km s^{-1}. The turbulent velocity width affects the effectiveness of the radiative excitation. However, since this is only of minor importance, we will use a constant value of 0.5 km s^{-1} throughout the envelope. The inner radius we set to 4 R_*; the stellar radius being estimated to be 4.5×10^{13} cm [we note here that Lopez et al. (1993) found the dust condensation radius to be about 6 R_*, where the dust temperature is $\sim$1000 K]. The inner parts of the CSE are complicated regions of which we have a very limited understanding, see e.g. Ryde et al. (1999), and where many of the basic assumptions of our model are certainly not valid. The properties of this region could, in principle, be of importance for the excitation of the higher rotational levels. According to our tests, however, an initial velocity gradient for example, affects the intensities only marginally. We have also performed tests showing that a change of the inner radius by a factor of two affects the derived FIR line intensities by at most a few percent.

The photodissociation radius of the CO envelope is defined as the location where the fractional abundance of CO is half the photospheric value. This was estimated to be 3.2×10^{17} cm for ^{12}CO (for the estimated mass loss rate) using the calculations by Mamon et al. (1988). The two isotopic variants have different photodissociation and chemical fractionation behaviour, but according to Mamon et al. (1988) these effects tend to cancel out, and the authors predict that the ^{12}CO/^{13}CO-ratio is constant with radius, except that the ^{13}CO envelope extends slightly further out. Here we assume the same radius for both isotopic variants. The J=1–0 lines are affected the most when varying the outer radius, but according to our calculations only by $\sim$20% in intensity, even if the outer radius is changed by a factor of two.

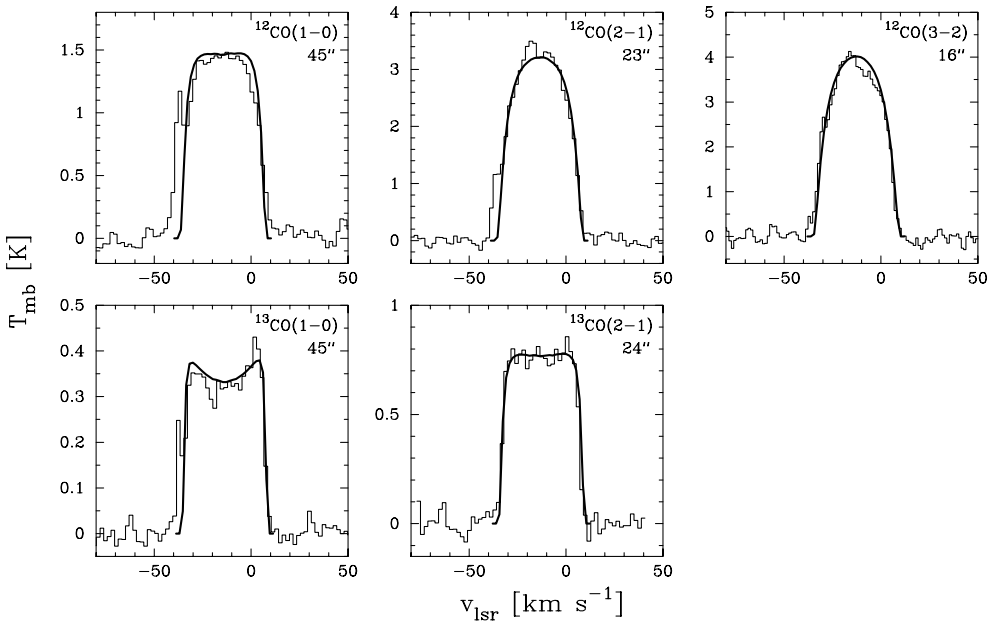

Fig. 2. Millimetre-wave CO spectra (histogram) observed towards IRAS 15194-5115 using SEST, overlaid with the best model results (full line) using a mass loss rate of $1\times10^{-5}\,M_\odot\,yr^{-1}$ and a $^{12}CO/^{13}CO$ ratio of 5.5. The beam size of each observation is given

We adopt an initial abundance of ^{12}CO with respect to H_2, f_{CO}, of 10^{-3}. The estimated mass loss rate scales roughly as $f_{CO}^{-0.8}$. The ^{13}CO abundance is obtained from the best-fit model.

4. Results and discussion

When running our model we vary the free parameters, the mass loss rate, the $^{12}CO/^{13}CO$-ratio, and the dust parameter h, until we get a good fit to the observed ^{12}CO and ^{13}CO radio line intensities, profiles, and radial brightness distributions (Nyman et al. 1993). This gives the kinetic temperature structure of the CSE, albeit constrained only by emission from the outer regions. Finally, we compare the model fluxes for the higher rotational transitions with our LWS observations. In Figs 2 & 3 we have plotted the line profiles (convolved with the instrumental resolutions) of the best-fit model to the ^{12}CO lines (there are narrow interstellar CO lines present in the blue wing of the radio lines, and we exclude these lines when integrating the radio fluxes). We also plot the best model fit to the ^{13}CO lines for the best estimate of the $^{12}CO/^{13}CO$-ratio.

From a simple error analysis, we arrive at a mass loss rate (based on the radio observations) of $(1\pm0.2)\times10^{-5}\,M_\odot\,yr^{-1}$ (excluding uncertainties in distance, ^{12}CO abundance, and the assumed circumstellar model), in agreement with other estimates (Nyman et al. 1993; Le Bertre 1997). We obtain a $^{12}CO/^{13}CO$-ratio of 5.5 ± 1. This result agrees excellently with that found by Nyman et al. (1993) using intensity ratios of isotopic variants of CS, CN, HCN, and HC_3N.

The kinetic and excitation (for selected transitions) temperature structures are plotted in Fig. 4. The ^{12}CO(1–0) transition is close to thermalised out to $\sim3\times10^{16}$ cm. The ^{13}CO(1–0) transition is strongly super-thermal in the inner parts, and it is never thermalised. The FIR lines are thermalised only out to about 1×10^{15} cm. The radio lines are formed mainly beyond $\sim5\times10^{16}$ cm ($\sim1000R_*$), corresponding to a time scale of $\gtrsim10^3$ yr, while the FIR lines are formed much closer to the star, within 10^{15} cm ($\sim10R_*$), which corresponds to $\lesssim20$ yr.

In Fig. 4 we also plot the radial variation of the various cooling terms included in the energy balance equation, Eq. (1). Here, for clarity, the cooling rate has been multiplied by a factor $\propto r^4$ (the heating due to dust-gas collisions goes roughly as r^{-4}). CO cooling (mainly by ^{12}CO) is the dominant coolant in the region between $\sim4\times10^{14}$ cm and $\sim1\times10^{17}$ cm, where most of the emission from the observed transitions emanates. In this context a high abundance of ^{13}CO could affect the modelled line intensities significantly. For IRAS 15194-5115 a $^{12}CO/^{13}CO$-ratio of only 5.5 implies that cooling by ^{13}CO could be as high as 20% of that of ^{12}CO. We have included ^{13}CO cooling in the same self-consistent way as for ^{12}CO and it turns out that its relative cooling is somewhat higher than 20%, Fig. 4, due to the fact that the lines of ^{13}CO are optically thinner than those of ^{12}CO. Closer to the star H_2 cooling dominates but very little emission from this part of the envelope contributes to the line emission observed. In the cool, tenuous, outer parts of the envelope, where most of the observed CO(1–0) emission arises, cooling due to the adiabatic expansion dominates.

We derive a dust parameter $h\sim2$ (with an estimated error of about 30%), i.e. twice as large as the one we used to fit the CO radio lines of IRC+10 216 in our modelling of this object. This indicates that the dust properties or the relative amount of dust could be different in the two objects. Our result is consistent with the finding by Groenewegen et al. (1998) in their dust models that IRAS 15194-5115 has a dust-to-gas ratio which is about twice the value for IRC+10 216 (using the same values for other dust parameters). However, our derived dust parameter is sensitive to the adopted luminosity, and hence the result is uncertain.

The model fluxes compare well with the observed FIR fluxes within the estimated errors, see Table 1, although we note that the fluxes from lines at longer wavelengths are systematically

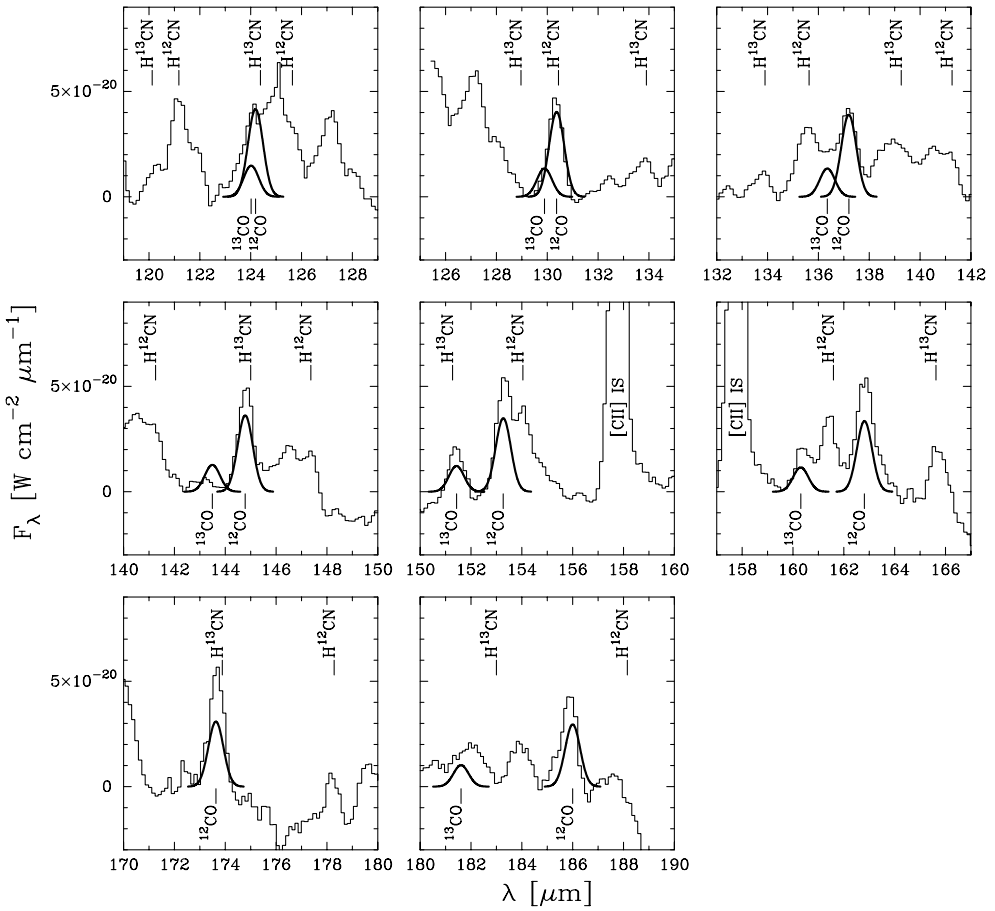

Fig. 3. Selected continuum-subtracted FIR CO spectra (histogram) observed towards IRAS 15194-5115 using the ISO satellite, overlaid with the best model results (full line) using a mass loss rate of 1×10^{-5} $M_\odot$ yr^{-1} and a $^{12}CO/^{13}CO$ ratio of 5.5. For all transitions the beam size and spectral resolution used are $70''$ and 0.7 μm, respectively

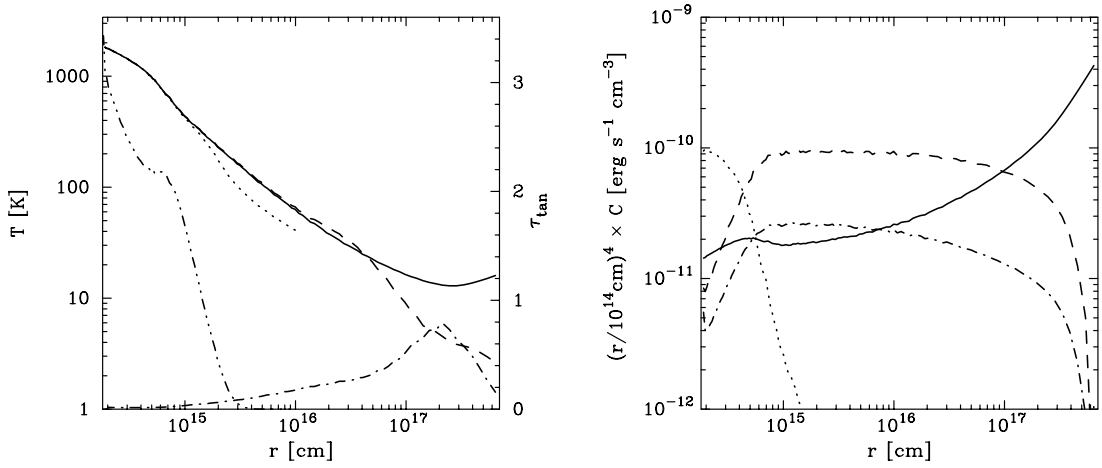

Fig. 4. The full line in the temperature panel gives the gas kinetic temperature, the dashed [dotted] line is the excitation temperature of the ^{12}CO(1–0) [^{12}CO(18–17)] transition. The dash-dot [dash-dot-dot-dot] line gives the tangential optical depth, $\tau_{\rm tan}$, of the ^{12}CO(1–0) [^{12}CO(18–17)] transition. In the cooling panel the full line represents adiabatic cooling; the dotted line the H_2 cooling; and the dashed line and the dash-dot line the ^{12}CO and ^{13}CO cooling, respectively (see text for details)

higher compared to what the model predicts, possibly indicating a systematic error. We conclude that the FIR data, probing the inner regions of the CSE, are consistent with the model derived from radio observations. Thus, we suggest that there have been no significant changes in the stellar wind characteristics over the past ∼5000 years. Due to the estimated large uncertainties in the LWS data the mass loss rate in the inner parts may have changed by about a factor of three and still be consistent with the model. Likewise, there appears to have been no significant change in the $^{12}CO/^{13}CO$-ratio over this period.

We believe that the circumstellar $^{12}CO/^{13}CO$-ratio is very close to the $^{12}C/^{13}C$-ratio in the stellar atmosphere. A $^{12}C/^{13}C$-

ratio of only 5.5 is just slightly larger than the equilibrium value of 3–3.5 found from hydrogen burning through the CNO-cycle. Such a low $^{12}C/^{13}C$-ratio puts IRAS 15194-5115 close to the group of C-stars known as the J-type stars, which have $^{12}C/^{13}C$-ratios of 3–4 (Lambert et al. 1986). Optically bright C-stars often have ratios above 30 (Lambert et al., 1986), and this seems to apply also for high mass loss rate objects (Greaves & Holland 1997). The best example of the latter is IRC+10 216 for which Kahane et al. (1992) derived a value of $^{12}C/^{13}C=44\pm3$. From its $^{12}C/^{13}C$-ratio IRAS 15194-5115 resembles more closely the extreme OH/IR-stars which are massive AGB stars in the very last phases of evolution (Delfosse et al. 1997). The low $^{12}C/^{13}C$-ratio of the OH/IR stars may be caused by hot bottom burning. This occurs when the temperature is larger than $\sim80\times10^6$K and this is only achieved in massive (5–8 $M_\odot$) AGB stars (Boothroyd et al., 1993). The luminosity derived for IRAS 15194-5115 from the period-luminosity relation ($8770\ L_\odot$) is, however, lower than typical OH/IR luminosities ($\sim3\times10^4\ L_\odot$). Thus, IRAS 15194-5115 may have been a J-star for which the $^{12}C/^{13}C$-ratio has remained low despite it probably being highly evolved. Alternatively, it may be a fairly massive star, which has recently become a carbon star due to quenching of hot bottom burning (Frost et al. 1998).

We have shown that modelling radio and FIR lines simultaneously is potentially an interesting diagnostic method for probing the stellar wind history of giant stars. Of special interest are, e.g., the group of OH/IR stars which are suggested to be undergoing an onset of a superwind phase with a drastically enhanced mass-loss rate during the recent 500–1000 years (Delfosse et al. 1997). This hypothesis could be observationally confirmed either with interferometric CO observations, as suggested by Delfosse et al. (1997) or by FIR observations of lines from rotationally excited CO molecules as is demonstrated in this paper.

Acknowledgements. We would like to thank L-Å Nyman for providing us with the radio observations, F. Kerschbaum and B. Larsson for discussions, and K. Eriksson and B. Gustafsson for providing valuable comments. E. Olsson is thanked for generous assistance. Support from the ISO Spectrometer Data Centre at MPE Garching, funded by DARA under grant 50 QI 9402 3 is acknowledged. The ISO Spectral Analysis Package (ISAP) is a joint development by the LWS and SWS Instrument Teams and Data Centers. Contributing institutes are CESR, IAS, IPAC, MPE, RAL and SRON.

References

Boothroyd A.I., Sackmann I.J., Ahern S.C., 1993, ApJ 416, 762
Cernicharo J., Barlow M., Gonzalez-Alfonso E., et al., 1996, A&A 315, L201
Chandra S., Maheshwari V., Sharma A., 1996, A&AS 117, 557
Clegg P., Ade P., Armand C., et al., 1996, A&A 315, L38
Crosas M., Menten K.M., 1997, ApJ 483, 913
Delfosse X., Kahane C., Forveille T., 1997, A&A 320, 249
Epchtein N., Le Bertre T., Lepine J.R.D., et al., 1987, A&AS 71, 39
Flower D.R., Launay J.M., 1985, MNRAS 214, 271
Frost C.A., Cannon R.C., Lattanzio J.C., Wood P.R., Forestini M., 1998, A&A 332, L17
Goldreich P., Scoville N., 1976, ApJ 205, 144
Greaves J.S., Holland W.S., 1997, A&A 327, 342
Groenewegen M.A.T., 1994, A&A 290, 531
Groenewegen M.A.T., Whitelock P.A., 1996, MNRAS 281, 1347
Groenewegen M.A.T., Whitelock P.A., Smith C.H., Kerschbaum F., 1998, MNRAS 293, 18
Kahane C., Cernicharo J., Gomez-Gonzalez J., Guelin M., 1992, A&A 256, 235
Kessler M.F., Steinz J.A., Anderegg M.E., et al., 1996, A&A 315, L27
Lambert D.L., Gustafsson B., Eriksson K., Hinkle K.H., 1986, ApJS 62, 373
Le Bertre T., 1992, A&AS 94, 377
Le Bertre T., 1997, A&A 324, 1059
Lopez B., Perrier C., Mekarnia D., Lefevre J., Gay J., 1993, A&A 270, 462
Mamon G.A., Glassgold A.E., Huggins P.J., 1988, ApJ 328, 797
Meadows P.J., Good A.R., Wolstencroft R.D., 1987, MNRAS 225, 43P
Nyman L.-Å., Olofsson H., Johansson L.E.B., et al., 1993, A&A 269, 377
Olofsson H., 1996, Ap&SS 245, 169
Ryde N., Eriksson K., Gustafsson B., 1999, A&A 341, 579
Swinyard B., Clegg P., Ade P., et al., 1996, A&A 315, L43